



OPEN

Exploring electronic structure of one-atom thick polycrystalline graphene films: A nano angle resolved photoemission study

José Avila¹, Ivy Razado¹, Stéphane Lorcy¹, Romain Fleurier², Emmanuelle Pichonat², Dominique Vignaud², Xavier Wallart² & María C. Asensio¹

¹Synchrotron SOLEIL, L'Orme des Merisiers, Saint Aubin-BP 48, 91192 Gif sur Yvette Cedex, France, ²IEMN, UMR CNRS 8520, Av. Poincaré, PO box 60069, 59652, Villeneuve d'Ascq Cedex, France.

Received
10 April 2013

Accepted
30 July 2013

Published
14 August 2013

Correspondence and
requests for materials
should be addressed to
M.C.A. (asensio@
synchrotron-soleil.fr)

The ability to produce large, continuous and defect free films of graphene is presently a major challenge for multiple applications. Even though the scalability of graphene films is closely associated to a manifest polycrystalline character, only a few numbers of experiments have explored so far the electronic structure down to single graphene grains. Here we report a high resolution angle and lateral resolved photoelectron spectroscopy (nano-ARPES) study of one-atom thick graphene films on thin copper foils synthesized by chemical vapor deposition. Our results show the robustness of the Dirac relativistic-like electronic spectrum as a function of the size, shape and orientation of the single-crystal pristine grains in the graphene films investigated. Moreover, by mapping grain by grain the electronic dynamics of this unique Dirac system, we show that the single-grain gap-size is 80% smaller than the multi-grain gap recently reported by classical ARPES.

Graphene, a two-dimensional honeycomb lattice of bonded carbon atoms, is a strong, stretchable and impermeable conducting membrane¹. It possesses chemical stability, optical transparency and extremely high carrier mobility among other surprising properties, however, these remarkable attributes are hardly exploited till reliable scalable graphene films could be attained². Mechanical exfoliation of graphite can produce high-quality graphene, but the size of the available flakes is rather small^{3,4}. Graphitization of SiC crystals and carbon evaporation on SiC substrates have successfully grown large-area of high quality graphene films^{5–9}; however, they are not easily transferable to arbitrary substrates and the thickness control is controversial, particularly when carbon-face SiC substrates are used.

Continuous graphene films can also be produced by diverse methods on metal substrates such as nickel, iridium, ruthenium among others^{10–14}. In most cases a mixed of mono- and bi-layer graphene has been reported¹⁵, with a variable hybridization between the metal and graphene states, depending on the substrate. Recently, Li and colleagues have produced centimetre scale one-atom thick graphene sheets by chemical vapor deposition (CVD) on copper foils¹⁶. Furthermore, by substrate etching the films have been transferred to alternative substrates, in a cost- and time-effective roll-to-roll production method¹⁷. Nonetheless, as the synthesis of scalable films production is attainable, the graphene films manifest their inherent polycrystalline character. Hence, recent high-resolution transmission microscopy studies have revealed the films as constituted by single-crystal grains differently oriented, which appear patched together like in a quilt¹⁸.

Bearing in mind that collective electronic excitations are at the heart of many open issues in graphene physics, it is essential to establish the impact of the polycrystalline nature on the low-energy quasiparticle behavior of graphene films¹⁹. Here we present ARPES data with high energy, momentum and lateral resolution obtained from monolayer graphene sheets grown on copper foils by CVD. Rather than individually imaging the atoms in each grain, we rapidly map at the mesoscopic scale the location, orientation and shape of several dozens of graphene and copper grains together with their grain boundaries. Thus, the vulnerability of the Dirac linear dispersion and the almost vanishingly mass of relativistic graphene carriers close to the Fermi level have been studied by nano-ARPES measurements of single pristine graphene grains as small as 4–6 μm size. More importantly, a deep nano-ARPES data analysis has allowed us to determine the lateral dependence (grain to grain) of relevant features like gap-size, doping, effective mass (m^*) and Fermi velocity (v_F) obtained by single- and multi-grains sampling.



Interestingly, even though the gap opening in graphene is usually discussed in terms of a semiconducting spectrum, where the occurrence of a finite gap at the Dirac point is accompanied by a measurable mass for the fermions. Our findings, reveal a gap scenario from graphene polycrystalline films, which preserves the massless characters of the carriers²⁰. Remarkably, nano-ARPES results have been able to unravel the discrepancies between recently reported experimental large gap-size of graphene on copper^{21,22} and theoretical predictions^{23–25}.

Results

Micro- and nano-ARPES measurements have been carried out at the ANTARES beamline^{26,27}, with lateral resolution of $\sim 90 \mu\text{m}$ and $\sim 120 \text{nm}$, respectively. This instrument, schematized in Fig. 1a, is particularly well suited to determine the electronic band structure of nano-sized samples as well as large specimens with nano heterogeneities²⁸. ARPES measurements are carried out under ultra-high vacuum conditions (with a base pressure better than 5×10^{-11} Torr), keeping the sample temperature as slow as $\sim 46 \text{K}$. Retaining the same lateral resolution as in nano-ARPES, the setup furthermore allows us a quantitative chemical analysis by detecting high-energy resolution core levels and their chemical shifts. The ANTARES microscope has two operating modes: (1) the point mode, in which individual electronic dispersion relations E-k curves can be measured with a nano- or micro-size sampling area, where E is the photoelectron binding energy and k the crystal-momentum, and (2) the scanning mode, wherein two-dimensional images can be

recorded by mapping the intensity of electronic states with selected values of momentum and binding energy. The overall energy and momentum resolution of the nano-ARPES measurements at 100 eV were 5 meV and 0.005\AA^{-1} , respectively.

Initially, we carry out a multi-grain study of the electronic structure by micro-ARPES measurements in the middle of sizable copper grains, which can be as large as 2 mm x1 mm, (see Fig. 1b and inset of Fig. 1c). Even if micro-ARPES measurements were conducted along an arbitrary direction (i.e., where the graphene π bands showed maximum intensity), a complete electronic band structure of a polycrystalline graphene film could be comprehensibly recognized, (see Fig. 1b). As the graphene grains, in principle, are almost randomly oriented, any arbitrary direction of the sample would coincide with the ΓK direction of grains of the graphene film investigated. Our findings show that strong graphene σ and π dispersing bands are clearly observed between 0.5 eV and 16 eV binding energies. Moreover, the region from about 2 eV to 4 eV is dominated by emission from the substrate valence band “d” copper states and finally close to the Fermi level, one finds the “sp” copper bands and the graphene π and π^* bands, which show a characteristic Dirac cone. The good valence band dispersion of the copper grains is indicative of the high crystalline quality of the copper substrate, despite its granular character. Interestingly, this typical electronic structure is distinctive of a rather weak interaction, with no evidence of hybridization between copper and graphene states, in line with previous studies^{29,30}.

Despite the absence of copper carbide formation, we have noticed that in the early stage of graphene growth, the interaction between

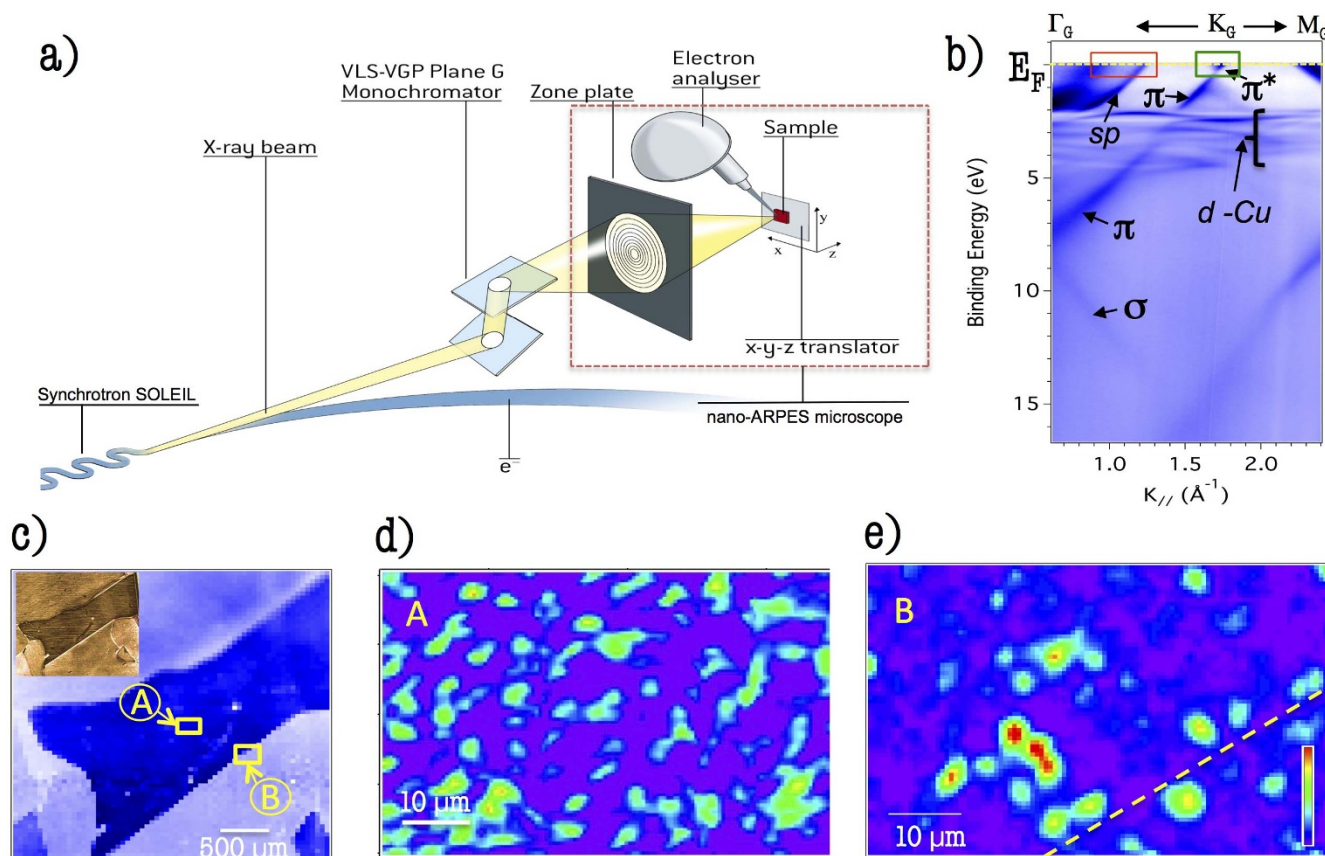


Figure 1 | Mixed real- and reciprocal-space images of a polycrystalline graphene film, grown on copper foils. (a) scheme of the nano-ARPES apparatus, connected to a beamline optics equipped with a focalization system composed by a pinhole, a Fresnel Zone plate and an Order Sorting Aperture (OSA). (b) micro-ARPES data inside one of a large copper grain of the sample. (c) real-space image of the copper states intensity (red box states of panel (b)) obtained by nano-ARPES mapping presented on a linear scale as a false-color image. The inset of panel (c) shows the optical image of the sample. Panels (d) and (e) show real-space images of graphene grains by monitoring the graphene states intensity (green box states of panel (b)) at the “A” and “B” yellow rectangles indicated in panel (c). Straight yellow dashed-line in panel (e) indicates the location of the corresponding Cu boundary grain.



the carbon source and the Cu substrate has played a quite important role, during the CVD synthesis. It seems that the extremely low carbon dissolvability in copper and the effective catalytic activity of the metallic substrate promoting the hydrocarbon gas decomposition are essential not only to ensure the growth of the one-atom thick graphene films but also to stimulate the growth of large and good crystalline copper grains of the substrate foils. In order to evaluate the influence of the granular nature of the substrate on the morphology of the graphene films, we have recorded nano-ARPES images by selectively mapping electronic states with a given binding energy and momentum.

In particular, by collecting exclusively the "sp" copper states (those confined in the red box of Fig 1b), the location, shape and orientation of Cu grains and their grain boundaries could be precisely determined. Figure 1c shows one of the resulting nano-ARPES images, in which a central grain presents an unusual Italian boot shape, similar to the one displayed by the optical microscope image (inset Fig. 1c). As we will discuss later on, these nano-ARPES images allow us moreover the unambiguous determination of the facet orientation of the copper substrate grains. If instead of copper states, we record the π^* states (green-box of Fig. 1b), the resulting nano-ARPES image provides the size, distribution and orientation of the graphene grains covering the copper grains, as can be observed in Figure 1d and 1e. In both graphene nano-ARPES images, the intensity of the π states graphene band is presented in a linear scale as a false-colour image. Both images recorded in the middle and at the border of the central copper grain, labelled as A and B-area in Fig. 1c, respectively, show similar shape and size distribution of the graphene grains inside and at the boundary substrate grains.

As the graphene π and π^* bands are only close to the Fermi level at the K points of the graphene grains investigated, the nano-ARPES image detects not only the presence of the pristine grains, but also their orientation (i.e., grains whose ΓK directions are collinear with the detector energy window). Accordingly, each nano-ARPES image provides the size and grain distributions in graphene films and the register with the copper substrate. Most importantly, once the individual graphene grains have been identified, we could investigate the properties associated to their individual Dirac cones. All recorded images independently of the grain orientation, depict a typical homogeneous distribution of dendritic graphene grains of 4–6 μm size, covering several copper grains as a carpet, without any observable disruption at the copper grain boundaries. As the images display only graphene grains of the same orientation, they suggest that the graphene films are discontinuous. Nevertheless, adding images of different orientations the whole graphene films could be reconstituted by pieces of pristine grains differently oriented, like a continuous patchwork fabric. Furthermore, if instead the π^* , the σ graphene bands are recorded, the nano-ARPES σ -derived images show an imperturbable continuity throughout the whole sample, disregarding the rich blend of grain orientations inherent to the polycrystalline graphene films. The σ -derived images have not been shown because they are black images, without any detectable contrast or intensity variation, confirming the continuity of the graphene films.

The cleanliness and spectroscopic quality of the CVD graphene films have been also investigated, before and after the ARPES measurements, by performing x-ray photoemission spectroscopy (XPS), scanning electron microscopy (SEM), optical imaging and Raman spectroscopy. Figure 2 shows a summary of our results. After exposure to the atmospheric pressure for several days, the samples were introduced in the ANTARES microscope and kept in ultra-high vacuum conditions. The level of contamination has been systematically evaluated by high-resolution core levels (CLs) measurements. As it can be seen in Fig. 2a, the as-grown films showed only a small oxygen contamination evidenced by a peak at binding energy ~ 550 eV. After a gentle annealing at 200°C , the Cu 3s, Cu 3d and C 1s photoelectron lines as well as the valence band were monitored.

The small initial oxygen contamination was easily removed by carrying out several cycles of annealing up to 600°C , as it can be seen in the Fig. 2a top spectrum.

Interestingly, high surface-sensitivity C 1s core level peaks resulting from the graphene films are dominated by a large main component, (see Fig. 1b). In addition a small shoulder appears at lower binding energies, which is associated probably to the presence of multi-layer graphene, which may behave as growth seeds. Special attention has been taken in order to ensure that our nano-ARPES samplings correspond exclusively to the large homogeneous single-layer areas of the samples. Typical monolayer graphene films display single peaks at 284.5 eV, without any evidence of a shoulder around 286–287 eV. Peaks appearing in this binding energy range have been considered as evidence of CO bondings or oxidized species in the samples. The absence of CO-derived peak indicates that the oxidized moieties generally detected during the synthesis or transfer steps have not produced measurable oxidation effects in the resulting graphene films. For a more quantitative analysis, we have fitted the XPS carbon CL 1s peak by a procedure involving the deconvolution of the peak with a Doniach and Sunjic³¹ line shape, using a Lorentzian line width of 170 meV and an asymmetry parameter of 0.068³². The C 1s level is found to have a lifetime full width half maximum (FWHM) with an upper limit of 170 ± 15 meV, which is considerably narrower than previously reported results^{33,34}, suggesting the existence of only one chemical environment of the carbon atoms.

The surface structure of graphene on Cu foil samples were also characterized by SEM imaging. Fig. 2c reveals the good homogeneity of the graphene film, with a mainly monolayer thick material while an insignificant part of the surface contains darker areas, which have been probably due to graphene growth seeds. Once the Cu surface is fully covered with graphene, the auto-limited growth of the films stops and consequently, the structure does not evolve any more. Moreover, as it is well known by Raman spectroscopy, we can distinguish easily between single-, few-layer graphene and graphite³⁵. The Raman fingerprint for single-layer graphene, is related directly to the position and G^2 -peak width. A narrow and intense Lorentzian G^2 -peak at ~ 2700 cm^{-1} is a direct signature of single-layer graphene, while broadening and blue-shift of the $2G^2$ -peak (with multiple Lorentzian lineshape) indicate multiple graphene layers. Figure 2d shows one of the typical Raman spectrum of the CVD graphene films investigated in this work. The G-peak at ~ 2700 cm^{-1} presents a FWHM of ~ 30 cm^{-1} and the IG^2/IG intensity ratio close to 2 (i.e. $IG^2/IG = 2$), which corresponds to the Raman fingerprints of single-layer graphene.

All the graphene films investigated in this study, have been grown immediately after the copper foils have been annealed up to $\sim 1050^\circ\text{C}$ under a mixture on argon and hydrogen flow. This treatment, together with carbon catalytic effect during the CDV growth induces a crystalline structure of the foil Cu grains predominantly dominated by the Cu (111) facet. This finding agrees well with theoretical predictions, as Cu (111) is the lowest energy copper surface³⁶, which has been corroborated recently by Electron backscattering diffraction³⁷, showing that the underlying copper foil substrates present large mono-crystalline copper grains Cu (111) faceted. Nevertheless, it is not clear yet if this almost epitaxial copper grain growth is the result of thermal treatment or due to a carbon catalytic effect¹⁸.

Figure 3a shows a typical LEED pattern measured in one of the large copper substrate grains of the graphene-copper-foil samples. According to graphene's six-fold symmetry, electron diffraction from a single graphene crystal should result in one set of six-fold symmetric spots arranged in a suitable honeycomb lattice, (see Fig. 3b). The LEED pattern of the samples, however, displays many of such families of spots, which give rise to a more or less continuous intensity ring. This is a consequence of the presence of several grains with different orientations in the field of view that the electron beam

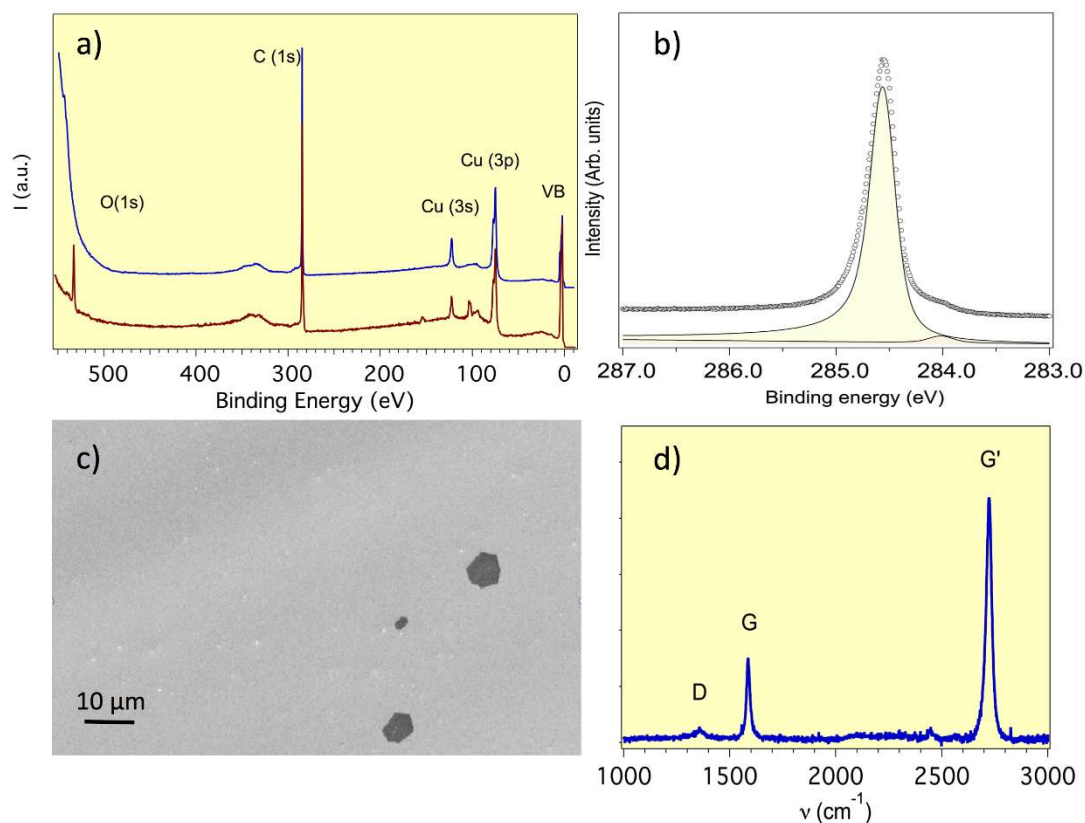


Figure 2 | (a) bottom line shows a typical XPS overview spectrum of graphene films grown by CVD on copper foils after air exposure for transfer purposes and a single 200°C one-hour annealing step. Top spectrum displays the same spectrum after the sample has been annealed up to 600°C, during 6 hours. (b) line-shape of C 1s photoelectron core level of the graphene film of panel (a), measured at the photon energy of 635 eV. (c) SEM image of graphene on a 50 μm thick copper foil. The image shows the presence of few graphene growth seeds (dark areas) together with dominant monolayer areas (light gray). (d) Raman spectra of a typical graphene film on copper foil. The small D peak ($\sim 1350\text{ cm}^{-1}$) and the intensity of the G' peak ($\sim 2700\text{ cm}^{-1}$) found to be more than twice as high as the G peak ($\sim 1580\text{ cm}^{-1}$) indicate the presence of high quality monolayer graphene.

is probing. Moreover, very close to the ring (Fig. 3a), a well-defined LEED set of six spot is observed. Their location in the reciprocal space corresponds to the high symmetry directions and size of the Brillouin zone of the Cu (111) grains. Indeed, the lattice parameters are 0.256 nm for the Cu (111) surface and 0.246 nm for graphene. So, there is a tensile strain of 4.1% for graphene on (111) Cu. Both graphene and copper grains features can be well distinguished in the figure inset, which shows a LEED pattern of the same sample taken with beam energy of 99 eV. The zoomed pattern shows that the

apparent copper (111) single spot is in fact composed by two very close speckles revealing the presence of two (111) copper domains, rotated 60° each other, similarly to previously reported metallic epitaxial growth³⁸. Figure 3b schematically shows the real and reciprocal lattice of individual and multiple pristine graphene grains randomly oriented, together with their corresponding Dirac cones associated to the π and π^* graphene bands.

The graphene-substrate registry is to a large extent disclosed, in Figure 4, by the multi-grain Fermi surface of the graphene-copper

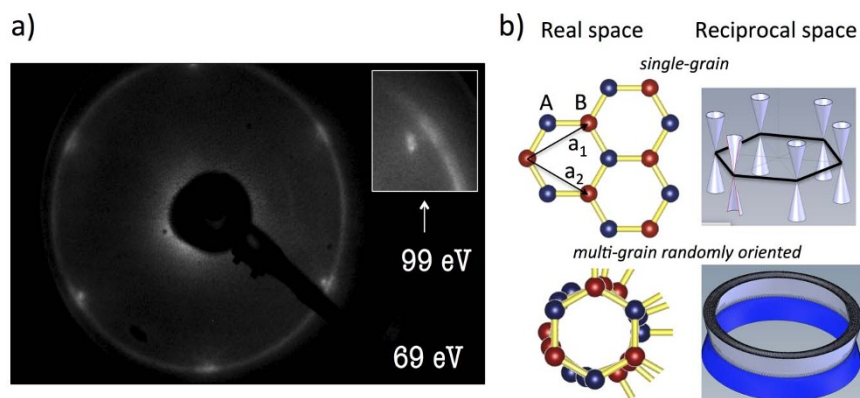


Figure 3 | (a) LEED pattern of a graphene film together with the six-fold single-crystal copper grain of the substrate. Panel (b) shows the real and reciprocal space of single- and multi- graphene grain. Moreover, the superposition of Dirac cones of graphene grains randomly oriented has been schematized.



samples collected in the sample area described by the A-box of Fig. 1. Bands coming from the copper substrate and the multi-grain graphene overlayer constitute the resulting Fermi surface map. Two sets of copper "sp" bands are clearly identified originated by the presence of two independent copper (111) domains, rotated 60° , in agreement with the LEED diffraction pattern of Fig. 3. Moreover, a large continuous circle, with a vector radius of $k_{\parallel} = 1.703 \text{ \AA}^{-1}$ is observed, which accounts for the contributions of the graphene π^* bands from different graphene pristine grains, (see Fig. 4c). A quantitative analysis of the circle intensity indicates that 60% of the graphene grains are preferentially oriented along the directions $\pm 3^\circ$ aside from the $[-110]$ direction of the Cu (111) surface, (see Fig. 4 c–e). These orientations labelled in Fig. 4c as β correspond to the most favorable matching between a six-fold graphene 2D lattice and a (111) copper grain.

Hence, the graphene one-atom thick film is made of pristine graphene islands and BGs, which are patched together as in a quilt, on granular copper foils constituted by large copper grains with (111) preferentially oriented crystalline structure. The graphene grains are single crystals with a robust fermion character, whose lattice and

consequently Dirac cones are rotated with respect to each other. The highly oriented graphene grains along preferential β directions coexist with grains randomly oriented along arbitrary directions labelled as α_n in Fig. 4c. This electronic structure description is in agreement with recent structural and morphologic microscopic studies^{37,39,18,40}.

In Figure 5, we compare the E-k dispersion of a multi-grain graphene film with the first (to our knowledge) high-resolution nano-ARPES Dirac-like dispersions of one-atom thick graphene grains of $\sim 4 \mu\text{m}$ size grown by CVD on copper foils. We have centred our study on the differences between the spectral function of single pristine graphene grains with different orientations and the one obtained probing simultaneously dozens of graphene grains, depicted in Fig. 5a,b and 5c, respectively. In agreement with previous graphene ARPES data, the photoemission intensity of one half of the Dirac cones is suppressed due to matrix elements effects, along ΓK directions when linear polarized photons have been used^{7,41,42}. In order to overcome these matrix elements effects, ARPES Dirac-like dispersion of multi-grain graphene films has also been measured using circularly polarized light, which does not present these matrix

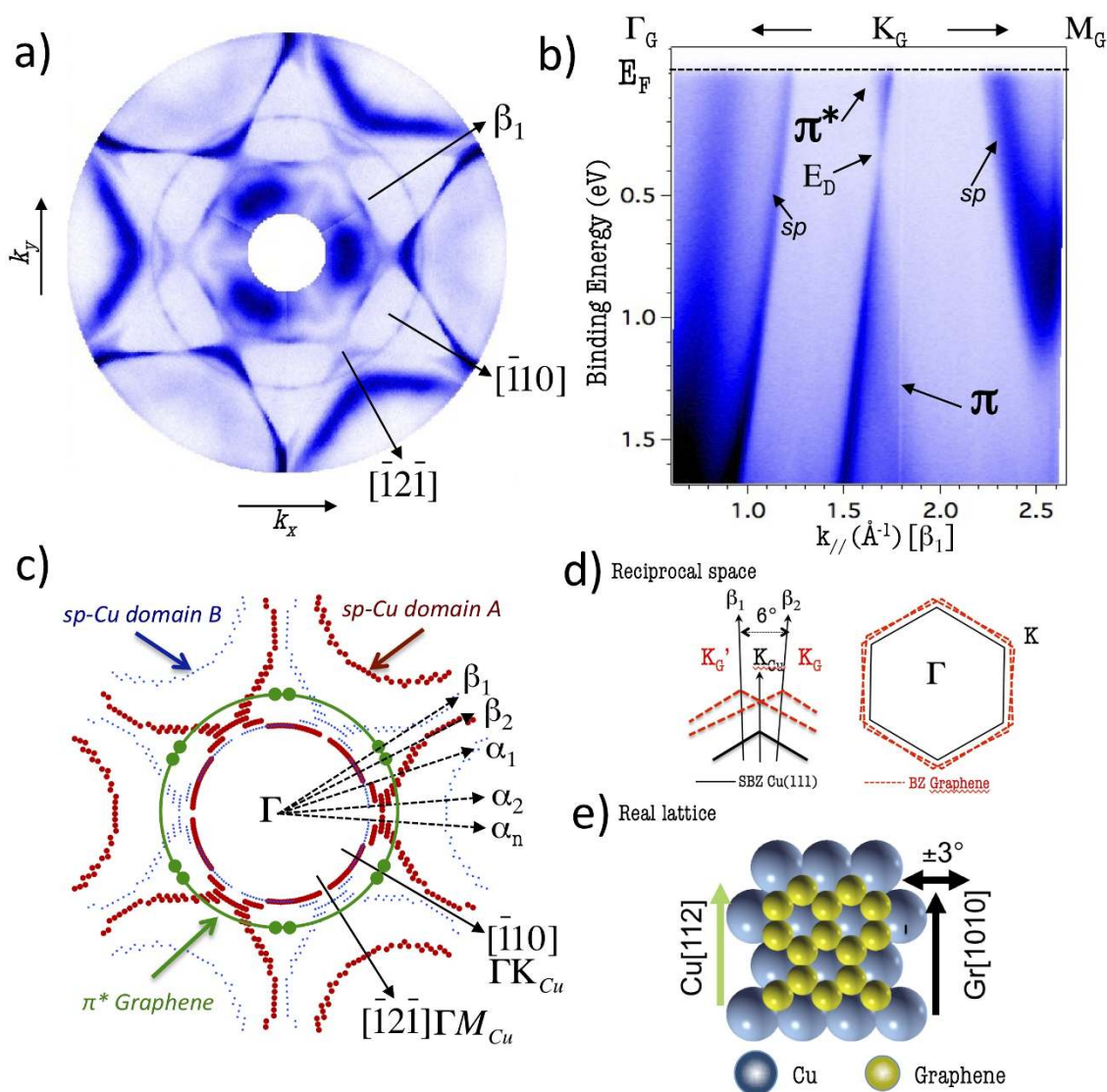


Figure 4 | Panel (a) shows the Fermi surface (FS) map of a graphene multi-grain film recorded at the B-box of figure 1c. Panel (b) displays the energy-momentum dispersion relations of π and π^* bands near E_F of graphene along the β direction, using linearly polarized light of 100 eV. A schematic diagram of the recorded FS is depicted in panel (c). Panel (e) depicts a sketch with the most favorable matching between the six-fold copper and graphene lattices.



element effects and consequently, both branches of the Dirac cone could be observed Fig. 5d.

ARPES results show, that both multi- and single-grain ARPES spectra present a well-defined conical Dirac dispersion, with n-type extrinsic doping (Fig. 5a–c). Moreover, from the Fermi momentum (k_F), that is the separation between the Dirac momentum at which the π^* band crosses the Fermi level, we have determined the average doping as a function of the grain orientation. Our findings show that the preferentially oriented grains are slightly more doped than randomly oriented ones. The typical extra charge of the β -oriented grains is $\sim 1.2 \times 10^{12} \text{ cm}^{-2}$, with a doping close to $n = 9.2 \times 10^{12} \text{ cm}^{-2}$, ($k_F = 0.054 \text{ \AA}^{-1}$ and $E_D = -0.371 \text{ eV}$, relative to the Fermi level). The spatial distribution of this charge within and at the border of the grains is out of the scope of the present work, thus it is being published elsewhere. Due to the continuous orientation distribution of the graphene grains, corroborated by LEED and the Fermi surface results, the multi-grain ARPES data, taken along any ΓK direction display "filled Dirac cones", (see Fig. 5d and 5e), which is a consequence of the Dirac cone overlapping from grains adjacently oriented.

Figure 6 shows ARPES data through a single Dirac cone along the ΓK direction. More precisely, the angle integrated photoemission intensity and Energy Distribution Curves (EDC), shown in panel

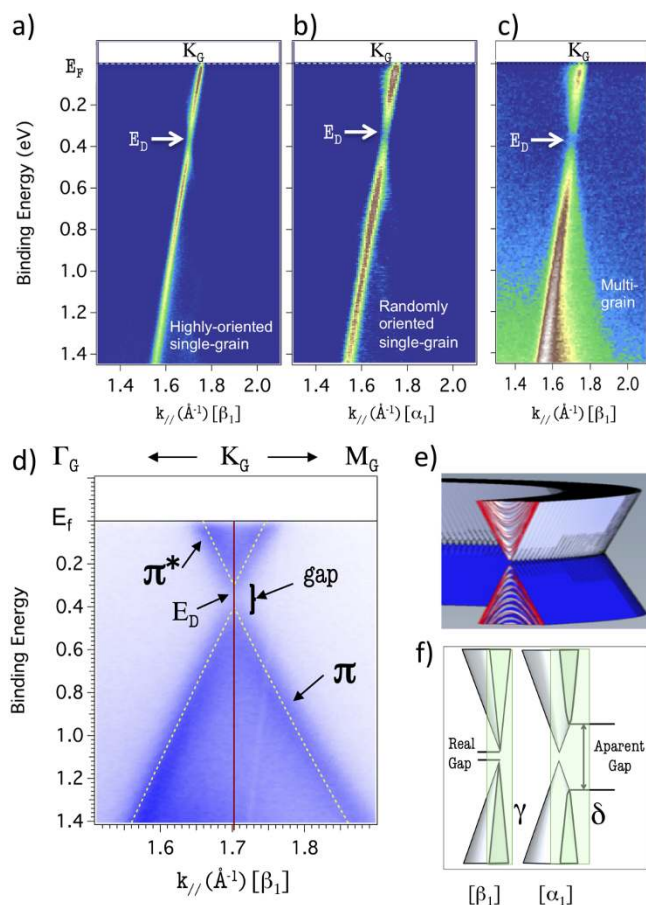


Figure 5 | Panel (a) and (b) show E-k dispersions measured by nano-ARPES in single pristine graphene grains oriented along the β and α directions, respectively, (see Fig. 4c). Panel (c) shows multi-grain E-k dispersion measured using micro-ARPES, along the β direction. Panel (d) displays the energy-momentum dispersion relations of π and π^* bands near E_F of multi-grain graphene film along the β direction, using circularly polarized light of 30 eV. Panel (f) depicts a schematic diagram representing the ARPES real and apparent gap at the Dirac point, depending on the γ - and δ - measurement plane, respectively.

(a) and (b–c) respectively, have been measured along the β_1 in Fig. 4c. This preferential orientation of the graphene domains is almost collinear with the ΓK_{Cu} direction, see Fig. 4 for more details. Discrete spectra show clearly that the photoemission intensity suppression along half of the cone due to matrix element effects⁴³. The EDCs of Fig. 6b–c show noticeably that the n-doped graphene bands present a bandgap minimum at the Dirac point. The existence of a gap creates two peaks in the EDCs at the K point (see black marks in (b) and (c) panels). As it has been extensively discussed in literature, the dispersion in the vicinity of the Dirac point has been subject of vigorous controversy, particularly in epitaxial graphene grown on Si-face of SiC single crystal substrates^{22,41}. The valence and conduction bands are not collinear, showing a region with minimum intensity between them. Whether or not this is due to the existence of a bandgap in the E-k dispersion or a many-body effect has been strongly debated for graphene on SiC substrates^{22,41}. For graphene on copper, however, the efficient dielectric screening of the metallic substrate excludes the possibility of electron-phonon coupling, and instead implies the existence of a bandgap at the Dirac point in graphene on copper foils.

Most importantly, a simple one-orbital tight binding (TB) analysis of the data allows us to evaluate the existence of a gap at the Dirac point. The nano-ARPES spectra from graphene single-grain were modelled by using a first nearest-neighbour TB based on the approach given by Saito et al.⁴⁴. The bare π -band dispersion $E_{\text{bare}}(k)$ was also computed using the TB model. We have in addition introduced the E_{gap} parameter to account for an energy gap at the Dirac energy, E_D . The first approximation band structure can be written as follow:

$$E_{\pi}(k) = \frac{\epsilon_{2p} \pm \gamma_0 \omega(k)}{1 \pm s_0 \omega(k)} \quad (1)$$

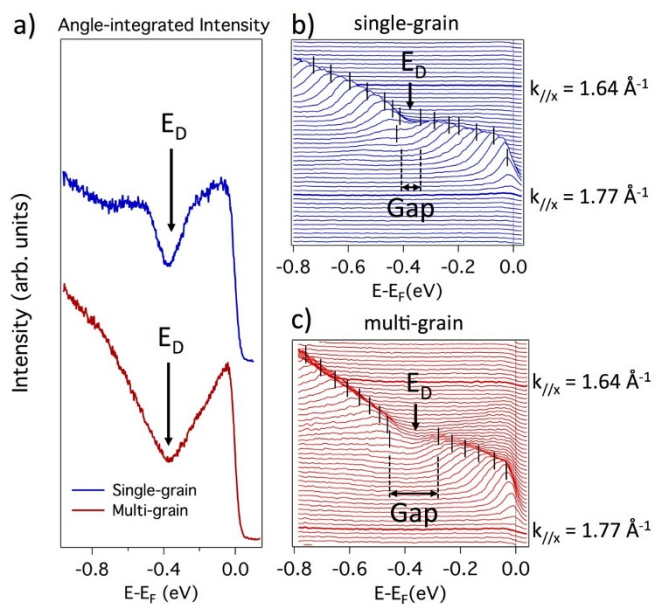


Figure 6 | Top and bottom curves of panel (a) show the angle-integrated photoemission spectrum of the single- and multi-grain, respectively, close to the Fermi level in a CVD graphene films grown on copper foil, along the β_1 direction, taken with an angular aperture of 25 degree. Features at the Dirac point and the size of the bandgap can be easily discerned. Panels (b) and (c) display EDCs along ΓK direction (coincident with the β_1 direction) in a single- and multi-grain graphene film, respectively. The n-doped graphene bands disclose clearly the minimum intensity at the Dirac point and the difference between the actual and apparent gap size described in the text.



$$\omega(k) = \sqrt{1 + 4\cos\left(\sqrt{3}ak_y/2\right)\cos(ak_x/2) + 4\cos^2(ak_x/2)} \quad (2)$$

where γ_0 and s_0 are the nearest neighbour hopping and overlap integrals, respectively. The data analysis allows us to conclude that all grains exhibit the opening of a mini-gap of 50 (± 5) meV at the Dirac point; which is more or less constant throughout the graphene film. This small gap is compatible with theoretical predictions and recent finding in graphene on metals, which calculated a gap of ~ 53 meV. This small gap opening can be rationalized as a consequence of a minor breaking of the graphene sub-lattice symmetry^{23–25,42,45}, due to a weak interaction with the substrate.

The best-fit parameters for the nearest neighbor hopping and overlap integrals are: $\gamma_0 = -3.24$ eV and $s_0 = 0.0425$ eV, respectively. Despite that we have used almost the same TB parameters as previous reported studies, the gap-size recorded by classical ARPES were up to 150% bigger than the single-grain gap reported in this work^{21,22}. A similar gap determination in our samples using multi-grain micro-ARPES (spot size ~ 90 μm) confirms as well an artificial enhancement of the gap up to a value of the order of ~ 150 (± 5) meV. Original spectra together with TB fitting parameters have been included in supplementary material available online.

The source of this artificial gap magnification is the rotational smearing of the spectral function due to azimuthal disorder of the sampled multi-grain films. As it can be seen in Figure 5f, the determination of the gap-size by ARPES requires the detection of the E-k dispersion precisely along the ΓK directions, (i.e. along the γ -plane in Fig. 5f). Hence, the gap energy value between the top and the bottom of the π and π^* bands, respectively, can be straightforward evaluated. This condition is easily fitted in classical ARPES if the samples are large mono-crystalline films. However, in polycrystalline samples, multi-grain sampling measurements record simultaneously signal from grains oriented differently. Consequently, while some grains are oriented along ΓK directions, we record considerable signal from grains with other orientations, which magnifies artificially the apparent gap due to the absence of states around the Dirac points because their E-k cone dispersions are measured in planes as the δ -planes, (Fig. 5f).

Discussion

By performing an in-depth analysis of the carrier interaction effects in extrinsic graphene grains (i.e., for doped graphene), we extract from nano-ARPES data the effective band velocity of the Dirac fermions in individual graphene grains. From the slope of the fitted dispersions, we extract the renormalized Fermi velocity, v_F^r , which is of the order of $\sim 1 \times 10^6$ m/s for all investigated grains. The momentum distribution function reflects the peculiar linear band structure of graphene, which deviates substantially from the usual parabolic metallic behaviour. Nevertheless, a more rigorous inspection reveals a rather distinctive renormalization depending on the orientation of the graphene grains. In particular, randomly oriented grains, which ΓK direction is collinear with α_n directions in Fig. 4c, present a strong deviation of the linearity, which induces a noticeable re-normalization of the Fermi velocity $v_F^r(\alpha) = (0.69 \pm 0.02) \times 10^6$ m/s. In preferentially oriented grains (collinear with β directions), however, the renormalization is weaker giving rise to a Fermi velocity of the order of $v_F^r(\beta) = (0.95 \pm 0.02) \times 10^6$ m/s. Therefore, the Fermi velocity of those grains oriented along the high symmetry direction of the copper substrate is almost 27% higher than the Fermi velocity of randomly oriented graphene grains.

Finally, we discuss another unusual feature related to graphene's relativistic-like spectrum. Our study reveals that even though the linear spectrum of fermions in graphene implies zero rest mass, the effective mass extracted by ARPES is not zero. For carrier densities of the order of $n \sim 8 \times 10^{12}$ cm^{-2} , the effective mass (m^*) is of the order of $\sim 0.066 m_e$ where m_e is the mass of the free electron, in

fairly good agreement with experimental cyclotron mass of exfoliated graphene^{3,46}. This effective mass value characterizes the grains preferentially oriented respect to the copper substrate, however, those grains randomly oriented present an effective mass of $m^* \sim 0.086 m_e$, almost 34% heavier than the highly oriented grains. As for the cyclotron mass, within the semi-classical approximation, the effective mass can be defined as a fictitious "relativistic" mass, $m^* = (k_F/v_F) \sqrt{n}$, which leads to $m^* = (\sqrt{\pi}/v_F) \sqrt{n}$, if the Fermi momentum k_F is expressed as a function of the electronic density n , considering that $n = k_F/\pi$. Fitting this equation to the experimental data provides estimation for the effective mass, which evidences for the existence of massless Dirac quasiparticles in graphene.

In summary, we have combined imaging graphene single-layer films with nano-ARPES measurements of the single-grain E-k dispersions to determine the robustness of the Dirac-like dispersion in polycrystalline graphene films grown by CDV synthesis. We have identified the size, doping and gap of graphene grains as a function of their orientation. Moreover, we have determined the register of graphene grains with the copper substrate lattice. Interestingly, we have been able to work out the lateral dependence (grain to grain) of the Dirac-like fermions properties, unravelling the relation between grain orientation, Fermi velocity and effective mass. More importantly, the nano-ARPES gap-size determination reveals the origin of the discordances between experimental gap-size values previously reported by classical ARPES and theoretical predictions, confirming that the graphene-copper interaction is rather weak, which gives rise to the opening of a mini-gap of the order of ~ 50 meV. Our findings, compatible with theoretical predictions and recent structural experimental reports, certainly open the door to a direct evaluation of the mesoscopic structure and its relation with the electronic properties of graphene films. Hence, by direct correlation between the single-grain electronic structure and the parameters of the CVD methods, nano-ARPES studies are able to provide key information on the optimal synthesis conditions of the graphene films and shed light on the electronic structure responsible of their chemical, optical and transport performance.

Methods

Chemical Vapor Deposition of graphene on copper foils. Copper foils were purchased from Alfa Aesar (50 μm thickness, 99.9995% purity). They were cut into 1×1 cm^2 pieces, and deoxidized using acetic acid, then rinsed in deionized water followed by acetone and isopropyl alcohol ultrasonic cleaning. They were then loaded into the CVD system, a cold-wall rapid-thermal processing set-up with a Si/SiO₂ susceptor fitted with an optical pyrometer. Cu pre-treatment includes a fast temperature gradient to $\sim 1050^\circ\text{C}$ followed by a 5 min annealing step under Ar (100 sccm) and H₂ (5 sccm) flow. Graphene growth was achieved at the same temperature, under CH₄ (20 sccm), H₂ (10 sccm) and Ar (100 sccm) flow (duration 5 min). The sample was then rapidly cooled under the same gas flow as the one used for the pre-treatment. The chamber pressure was set to 10 torrs. The annealing pre-treatment of the Cu foils leads to large and well ordered crystalline grains as large as 2×1 mm^2 (see optical micrographs in Fig. 1c). Combining scanning and point mode nano-ARPES in a reference pre-treated only Cu sample, we have observed that the foils are composed almost exclusively of large single-crystal grains with a (111) surface with some in-plane tilt between grains. Only in rare occasions, they show a measurable small tilt from the (111) orientation. Our findings are consistent with results reporting on the most stable morphology and crystallinity of textured copper foils.

Nano Angle Resolved Photoelectron Spectroscopy (nano-ARPES). Most of the photoemission experiments (PES) were performed with a photon energy $h\nu = 100$ eV and linearly horizontal polarized light at a base pressure better than 5×10^{-11} Torr and keeping the sample temperature at ~ 46 K. Moreover, in order to sort out problems originated from the photoemission selection rules or "dark corridor" along the ΓK direction, we have also performed PES experiments using circularly polarized light photon energy $h\nu = 30$ eV. The ANTARES microscope is equipped with the Scienta R4000 hemispherical electron analyzer with a detection system based on a 40 mm diameter multi-channel plate (MCP) detector. The wide-angle lens of the detector allows a fast and accurate band mapping and XPS/UPS measurements. The lens set with an acceptance angle of 25° or 14° has excellent angular and transmission properties. The Nano-ARPES setup is fully automatically controlled by a complete Tango based software. Both the data acquisition and the communication with external devices are piloted by a unique user friendly code.



The nano-ARPES microscope of the Antares beamline is equipped with two Fresnel zone plates (FZP; i.e. for low and high photon energy) responsible of the synchrotron radiation beam focalization and an order selection aperture (OSA) to eliminate higher diffraction orders. Moreover, the samples are mounted on a nano-positioning stage placed at the coincident focus of the Scienta analyzer and the FZP focal point, which is responsible of the sample rastering during the image acquisition. The spatial resolution is determined by the FZP resolution and the mechanical stability of the sample stage. This innovative instrument is therefore well suited to determine the electronic band structure of nano-sized samples as well as large specimens with nano-heterogeneities by using ARPES. The studies can be consistently completed with a quantitative chemical analysis detecting high-energy resolution core levels along with the chemical shifts of the investigated samples, keeping the same spatial resolution as in nano-ARPES. The ANTARES microscope has two operating modes, the point mode, where an individual ARPES detection can be done in a nano- or micro-area of the sample and a scanning mode, which by mapping the intensity of electronic states of a given momentum and binding energy throughout the samples, it is possible to generate two-dimensional images of a particular electronic feature.

- Castro Neto, A. H., Peres, N. M. R., Novoselov, K. S. & Geim, A. K. The electronic properties of graphene. *Rev. Mod. Phys.* **81**, 109–162 (2009).
- Avouris, P., Chen, Z. & Perebeinos, V. Carbon-based electronics. *Nat. Nanotechnol.* **2**, 605–615 (2007).
- Novoselov, K. S. *et al.* Two-dimensional gas of massless Dirac fermions in graphene. *Nature* **438**, 197–200 (2005).
- Meyer, J. C. *et al.* The structure of suspended graphene sheets. *Nature* **446**, 60–63 (2007).
- Berger, C. *et al.* Electronic confinement and coherence in patterned epitaxial graphene. *Science* **312**, 1191–1196 (2006).
- Hwang, C. *et al.* Fermi velocity engineering in graphene by substrate modification. *Sci. Rep.* **2**, 590; doi:10.1038/srep00590 (2012).
- Bostwick, A., Ohta, T., Seyller, T., Horn, K. & Rotenberg, E. Quasiparticle dynamics in graphene. *Nat. Phys.* **3**, 36–40 (2006).
- Siegel, D. A. *et al.* Many-body interactions in quasi-freestanding graphene. *Proc. Natl. Acad. Sci.* **108**, 11365–11369 (2011).
- Moreau, E. *et al.* Graphene growth by molecular beam epitaxy on the carbon-face of SiC. *Appl. Phys. Lett.* **97**, 241907 (2010).
- N'Diaye, A. T., Coraux, J., Plasa, T. N., Busse, C. & Michely, T. Structure of epitaxial graphene on Ir(111). *New J. Phys.* **10**, 043033 (2008).
- Vazquez de Parga, A. L. *et al.* Periodically rippled graphene: growth and spatially resolved electronic structure. *Phys. Rev. Lett.* **100**, 56807 (2008).
- Coraux, J. *et al.* Growth of graphene on Ir(111). *New J. Phys.* **11**, 039801 (2009).
- Sutter, P. W., Flege, J. I. & Sutter, E. A. Epitaxial graphene on ruthenium. *Nat. Mater.* **7**, 406–411 (2008).
- Pletikoscic, L. *et al.* Dirac Cones for Graphene on Ir(111). *Phys. Rev. Lett.* **102**, 056808 (2009).
- Reina, A. *et al.* Growth of large-area single- and Bi-layer graphene by controlled carbon precipitation on polycrystalline Ni surfaces. *Nano Res.* **2**, 509–516 (2010).
- Li, X. Large-Area Synthesis of High-Quality and Uniform Graphene Films on Copper Foils. *Science* **324**, 1312 (2009).
- Bae, S. *et al.* Roll-to-roll production of 30-inch graphene films for transparent electrodes. *Nat. Nanotechnol.* **5**, 574–578 (2010).
- Rasool, H. I. *et al.* Continuity of Graphene on Polycrystalline Copper. *Nano Lett.* **11**, 251–256 (2011).
- Yazyev, O. V. & Louie, S. G. Electronic transport in polycrystalline graphene. *Nat. Mater.* **9**, 806–809 (2010).
- Zhou, S. Y. *et al.* Substrate-induced bandgap opening in epitaxial graphene. *Nat. Mater.* **6**, 916–916 (2007).
- Walter, A. *et al.* Electronic structure of graphene on single-crystal copper substrates. *Phys. Rev. B* **84**, (2011).
- Siegel, D. A., Hwang, C., Fedorov, A. V. & Lanzara, A. Electron–phonon coupling and intrinsic bandgap in highly-screened graphene. *New J. Phys.* **14**, 095006 (2012).
- Giovannetti, G., Khomyakov, P., Brocks, G., Kelly, P. & van den Brink, J. Substrate-induced band gap in graphene on hexagonal boron nitride: Ab initio density functional calculations. *Phys. Rev. B* **76**, 073103 (2007).
- Khomyakov, P. A. *et al.* First-principles study of the interaction and charge transfer between graphene and metals. *Phys. Rev. B* **79**, 195425 (2009).
- Varykhalov, A., Scholz, M. R., Kim, T. K. & Rader, O. Effect of noble-metal contacts on doping and band gap of graphene. *Phys. Rev. B* **82**, 121101 (2010).
- Avila, J. *et al.* ANTARES, a scanning photoemission microscopy beamline at SOLEIL. *JPCS.* **425**, 192023 (2013).
- Avila, J. *et al.* Interferometer-controlled soft X-ray scanning photoemission microscopy at SOLEIL. *JPCS.* **425**, 132013 (2013).
- Bostwick, A., Rotenberg, E., Avila, J. & Asensio, M. C. Zooming in on Electronic Structure: NanoARPES at SOLEIL and ALS. *Synchrotron Radiat. News* **25**, 19–25 (2012).
- Dedkov, Y., Fonin, M., Rüdiger, U. & Laubschat, C. Rashba Effect in the Graphene/Ni(111) System. *Phys. Rev. Lett.* **100**, (2008).
- Marchini, S., Günther, S. & Wintterlin, J. Scanning tunneling microscopy of graphene on Ru (0001). *Phys. Rev. B* **76**, 075429 (2007).
- Doniach, S. & Sunjic, M. Many-electron singularity in X-ray photoemission and X-ray line spectra from metals. *J. Phys. C Solid State Phys.* **3**, 285–291 (1970).
- Prince, K. *et al.* Core-level photoemission from graphite. *Phys. Rev. B* **62**, 6866–6868 (2000).
- Kim, K. *et al.* Scanning photoemission microscopy of graphene sheets on SiO₂. *Adv. Mater.* **20**, 3589–3591 (2008).
- Lim, H. *et al.* Unique photoemission from single-layer graphene on a SiO₂ layer by a substrate charging effect. *Chem. Commun.* **47**, 8608 (2011).
- Malard, L. M., Pimenta, M. A., Dresselhaus, G. & Dresselhaus, M. S. Raman spectroscopy in graphene. *Phys. Reports* **473**, 51–87 (2009).
- Chatain, D., Ghetta, V. & Wynblatt, P. Equilibrium Shape of Copper Crystals Grown on Sapphire. *Interface Sci.* **12**, 7–18 (2004).
- Wood, J. D., Schmucker, S. W., Lyons, A. S., Pop, E. & Lyding, J. W. Effects of Polycrystalline Cu Substrate on Graphene Growth by Chemical Vapor Deposition. *Nano Lett.* **11**, 4547–4554 (2011).
- Sánchez-Royo, J., Avila, J., Pérez-Dieste, V., De Seta, M. & Asensio, M. Two-domains bulklike Fermi surface of Ag films deposited onto Si(111)-(7 × 7). *Phys. Rev. B* **66**, 035401 (2002).
- Nie, S., Wofford, J., Bartelt, N., Dubon, O. & McCarty, K. Origin of the mosaicity in graphene grown on Cu(111). *Phys. Rev. B* **84** (2011).
- Chen, H., Zhu, W. & Zhang, Z. Contrasting Behavior of Carbon Nucleation in the Initial Stages of Graphene Epitaxial Growth on Stepped Metal Surfaces. *Phys. Rev. Lett.* **104** (2010).
- Bostwick, A. *et al.* Observation of Plasmarons in Quasi-Freestanding Doped Graphene. *Science* **328**, 999–1002 (2010).
- Pletikoscic, I., Kralj, M., Milun, M. & Pervan, P. Finding the bare band: Electron coupling to two phonon modes in potassium-doped graphene on Ir(111). *Phys. Rev. B* **85**, 155447 (2012).
- Shirley, E. L., Terminello, L. J., Santoni, A. & Himpel, F. J. Brillouin-zone-selection effects in graphite photoelectron angular distributions. *Phys. Rev. B* **51**, 13614 (1995).
- Grüneis, A. *et al.* Tight-binding description of the quasiparticle dispersion of graphite and few-layer graphene. *Phys. Rev. B* **78**, 205425 (2008).
- Kralj, M. *et al.* Graphene on Ir (111) characterized by angle-resolved photoemission. *Phys. Rev. B* **84**, 075427 (2011).
- Zhang, Y., Tan, Y. W., Stormer, H. L. & Kim, P. Experimental observation of the quantum Hall effect and Berry's phase in graphene. *Nature* **438**, 201–204 (2005).

Acknowledgments

The authors acknowledge Yves Petroff and Petar Pervan for useful discussions. The authors also thank J.-L. Giorgetta, J.-O. Forsell and F. Polack, for the design of the ANTARES beamline and the nano-ARPES microscope. We also acknowledge Tolek Tyliczszak and Adam P. Hitchcock for your help. The Synchrotron SOLEIL is supported by the Centre National de la Recherche Scientifique (CNRS) and the Commissariat à l'Énergie Atomique et aux Énergies Alternatives (CEA), France.

Author contributions

R.F., E.P., D.V. and X.V. carried out the growth of the samples and RAMAN characterization. J.A., I.R., S.L. and M.C.A. performed the ARPES experiments. J.A. and M.C.A. have conducted the research design and data analysis. This manuscript was written by M.C.A. All authors discussed the results and commented on the manuscript.

Additional information

Supplementary information accompanies this paper at <http://www.nature.com/scientificreports>

Competing financial interests: The authors declare no competing financial interests.

How to cite this article: Avila, J. *et al.* Exploring electronic structure of one-atom thick polycrystalline graphene films: A nano angle resolved photoemission study. *Sci. Rep.* **3**, 2439; DOI:10.1038/srep02439 (2013).



This work is licensed under a Creative Commons Attribution-NonCommercial-NoDerivs 3.0 Unported license. To view a copy of this license, visit <http://creativecommons.org/licenses/by-nc-nd/3.0>